applied sciences

MDPI

Article

Small-Signal Stability Analysis and Improvement in Multi-Converter Grid-Tied System Based on Gerschgorin Disc Theorem

Bo Chen [1], Qi Si [2,*], Pan Jiang [2] and Xiaojuan Zhu [2]

[1] Electric Power Research Institute of State Grid Jiangxi Electric Power Co., Ltd., Nanchang 330096, China; orchis1986@126.com
[2] School of Electrical Engineering, Southwest Jiaotong University, Chengdu 611756, China; jiangpan@my.swjtu.edu.cn (P.J.); zhuxjswjtu@163.com (X.Z.)
* Correspondence: s2018112358@my.swjtu.edu.cn

Abstract: The integration of a large number of voltage source converters (VSCs) into the power grid decreases the small-signal stability of the power system. When several VSCs with different control parameters are simultaneously connected to the power grid to form a multi-converter grid-tied system, the potential destabilizing factors increase. Thus, parameter optimization for stability-weakest parameters that have the greatest impact on the system stability becomes more significant in addressing small-signal stability issues. This paper first proposes a stability evaluation function based on the Gerschgorin disc theorem, which can assess the stability of the multi-converter grid-tied system. Then a parameter sensitivity method is proposed to identify the stability-weakest parameters. Finally, an iterative calculation-based parameter optimization method is developed to regulate the identified stability-weakest parameters. Hence, the parameter optimization technique in this research can improve the system stability without requiring eigenvalue solutions and has the merit of low computational complexity. Simulation results based on both the MATLAB/Simulink (2023a) and the RT-LAB (OPAL-RT 5700) platform of a multi-converter grid-tied system validate the correctness of the theoretical analysis and the effectiveness of the parameter optimization method.

Keywords: multi-converter grid-tied system; stability-weakest parameters; identification; Gerschgorin disc theorem; parameter optimization

Citation: Chen, B.; Si, Q.; Jiang, P.; Zhu, X. Small-Signal Stability Analysis and Improvement in Multi-Converter Grid-Tied System Based on Gerschgorin Disc Theorem. *Appl. Sci.* **2024**, *14*, 1436. https://doi.org/10.3390/app14041436

Academic Editors: Federico Barrero and Mario Bermúdez

Received: 29 November 2023
Revised: 20 January 2024
Accepted: 29 January 2024
Published: 9 February 2024

1. Introduction

The promotion of new energy generation has become a global consensus to address the energy crisis and environmental pollution [1,2]. An increasing number of power-electrolyzed sources and loads, such as wind power, photovoltaics (PV), and flexible load, are connected to power systems through voltage source converters (VSCs) [3–5]. However, the wide-frequency dynamic characteristics of VSCs can easily interact with the power grid, leading to small-signal instability in the system [6–8]. In a multi-converter grid-tied system especially, the interaction between the power grid and VSCs becomes more intense, leading to increased potential instability factors and further exacerbating the risk of system instability.

Currently, the concepts and discussions on the small-signal stability issue of the multi-converter grid-tied system have been well established. Optimizing the control parameters of VSC is an effective method to improve system stability. Existing parameter optimization can be mainly divided into two categories: the direct method [9–11] and the sensitivity-based parameter optimization method [12–15].

The direct method of parameter optimization is to substitute specific values into the impedance model of the VSC and observe the influence of control parameter changes on the system stability to identify the patterns of parameter variations. Based on this law,

parameter optimization is carried out to achieve system stability [9,10]. The patterns of parameter variations obtained by substituting specific numerical values may be not applied to parameter optimization for operating conditions with different parameter combinations. A universal parameter optimization method is proposed in [11] based on an analytical method used to uniformly analyze the influence of control parameters on the sequence impedance of grid-forming converters. However, the impact of parameter changes on the stability of a single-converter grid-tied system is analyzed but cannot guide the parameter optimization of a multi-converter grid-tied system. The direct method can only optimize parameters by qualitatively analyzing the impact of VSC control parameter changes on system stability, lacking theoretical support.

The sensitivity-based parameter optimization method is to optimize parameters by quantitatively analyzing the influence of variables on system stability [12]. Then, the parameter optimization is carried out on this basis. The ports [13], subsystems [13], or state variables [14] that have the greatest impact on system stability can be identified by using participation factors. Then, only the parameters related to ports, subsystems, or state variables need to be analyzed, reducing the range of parameters that may be used for parameter optimization. A parameter optimization method is proposed based on parameter sensitivity analysis [15]. Through quantitative analysis of the influence of each VSC parameter on the system stability, the stability-weakest parameters are identified, that is, the parameter that had the greatest impact on the system stability. This method could minimally change the stability-weakest parameters to improve the system stability. However, this method still needed to be tried step by step for the optimization of stability-weakest parameters and could not provide specific parameter optimization values.

In the current parameter optimization of the multi-converter grid-tied system, it is challenging to provide specific recommendations of control parameters for different units to improve the system stability. The current parameter optimization can only analyze the impact of parameter changes on system stability, and lacks specific quantitative parameter optimization goals. Specific parameter optimization values cannot be obtained directly. Naturally, the targeted theoretical guidance for enhancing system stability is insufficient. Overall, the above discussions motivate us to propose a new method in this article to optimize stability-weakest parameters to improve the stability of the multi-converter grid-tied system. The major contributions and innovations of this research are reflected in the following three aspects:

(1) Proposing a stability evaluation function for a multi-converter grid-tied system based on the Generalized Nyquist Criterion (GNC) and the Gerschgorin disc theorem, which provides an intuitive quantitative indicator for estimating system stability. By considering the distance between the fastest intersection of the Gerschgorin disc with the real axis and the point $(-1, j0)$, the stability evaluation function in this paper can overcome the misjudgment in parameter optimization direction caused by the change in the Gerschgorin disc's radius due to parameter variation.
(2) By using the derivative operation among the control parameters of VSCs and the stability evaluation function, numerical results that characterize the impact of VSCs control parameters on system stability are obtained. The parameters with large absolute sensitivity values are identified as stability-weakest parameters.
(3) Developing a stability-weakest parameters-based optimization method by iterative calculation, which can calculate the specific control parameter optimization value to improve the system stability. It can compensate for the theoretical shortcomings of traditional methods, i.e., that parameter optimization can only be attempted step by step and lacks targeted theoretical guidance for the optimization of VSCs control parameters.

The rest of this article is organized as follows. Section 2 deduces the impedance model of the multi-converter grid-tied system. Section 3 uses the GNC and the Gerschgorin disc theorem to establish a stability evaluation function for the system. Additionally, it proposes a method of parameter optimization based on the parameter sensitivity analysis. Section 4

elaborates on the simulation results to validate the effectiveness of the proposed method. Finally, Section 5 summarizes the conclusions and contributions of this article.

2. Impedance-Based Model of Multi-Converter Grid-Tied System

2.1. Equivalent Model of VSC

Figure 1 illustrates the system structure of the VSC controlled in the *dq* frame. In Figure 1, V_{dc} is a DC voltage source. L_f is the filter inductance. L_g is the grid impedance. U_g is the grid voltage. u_{pcc} is the point of common coupling (PCC) voltage. u_{pccdq} are the PCC voltage in the *dq* frame. θ_{pll} is the output angle of the phase-locked loop (PLL). $H_{pll} = k_{pllp} + k_{plli}/s$ is a proportional-integral (PI) controller, where k_{pllp} is the proportional coefficient and k_{plli} is the integral coefficient. i_o is the output current of the VSC. i_{odq} are the PCC current in the *dq* frame. I_{dqref} are the instruction reference values in the *dq* frame. I_{dqref} are controlled by a PI controller $H_{ci} = k_{ip} + k_{ii}/s$, where k_{ip} is the proportional coefficient and k_{ii} is the integral coefficient. v_{mdq} are the modulation signals output by current loop control in the *dq* frame.

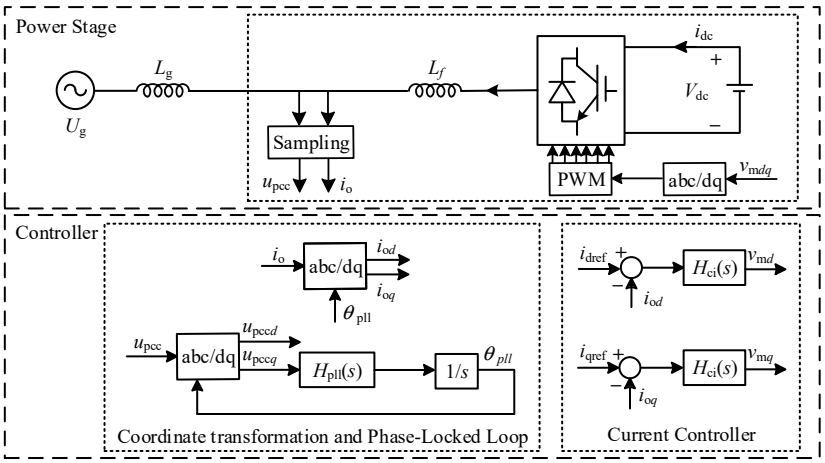

Figure 1. Structure diagram of VSC controlled in *dq* frame.

In this article, the frequency range considered is within 1000 Hz which is much smaller than the switching frequency of VSC. Therefore, pulse-width modulation (PWM) can be approximated as a linear element [16]. v_{mdq} can be written as follows:

$$v_{md} = \frac{u_{pccd} - \omega_1 L_f i_q}{K_{PWM}} \tag{1}$$

$$v_{mq} = \frac{\omega_1 L_f i_d + u_{pccq}}{K_{PWM}} \tag{2}$$

where K_{PWM} is the proportional gain of the PWM. ω_1 is the fundamental frequency of the power grid.

The PLL is used to obtain the amplitude and phase information of the grid voltage and ensure the synchronous operation of the VSC and the power grid. When small-signal perturbations are added to the grid voltage, the system *dq* frame defined by the grid voltage and the controller *dq* frame defined by the PLL do not align with each other. Therefore, the state variables in the system *dq* frame and the state variables in the controller *dq* frame need to be unified through a coordinate transformation. The relationship between the state variables in the system *dq* frame, controller *dq* frame, and the phase difference $\Delta\theta$ can be deduced:

$$\begin{cases} \Delta\gamma_{d,s} = \Delta\gamma_{d,c} - \Delta\theta\gamma_{q0,s} \\ \Delta\gamma_{q,s} = \Delta\gamma_{q,s} + \Delta\theta\gamma_{d0,s} \end{cases} \tag{3}$$

where γ denotes the state variables such as voltage, current, and duty cycle. Δ represents the fluctuation signals. The d and q in the subscript represent the state variables in the d-axis and q-axis, respectively. The 0 in the subscript represents the steady state of the state variables. The s and c at the end of the subscript represent the state variables in the system dq frame and the controller dq frame, respectively.

Combined with the Equation (3) and the PLL model shown in Figure 1, the PLL output angle can be derived as

$$\Delta\theta = \frac{H_{\mathrm{PI}}(s)}{s + H_{\mathrm{PI}}(s)U_{\mathrm{pccd0},s}}\Delta u_{\mathrm{pccq},s} \tag{4}$$

where $U_{\mathrm{pccd0},s}$ is numerically equal to the phase voltage amplitude of the power grid. s is the Laplacian operator.

Substituting Equation (4) into Equation (3), the transformation relationship between the variables in two dq frames can be represented by

$$\begin{bmatrix}\Delta\gamma_{d,s}\\ \Delta\gamma_{q,s}\end{bmatrix} = \begin{bmatrix}\Delta\gamma_{d,c}\\ \Delta\gamma_{q,c}\end{bmatrix} + \begin{bmatrix}0 & -\frac{H_{\mathrm{pll}}(s)\gamma_{q,s}}{s+H_{\mathrm{pll}}(s)U_{pccd0,s}}\\ 0 & \frac{H_{\mathrm{pll}}(s)\gamma_{d,s}}{s+H_{\mathrm{pll}}(s)U_{\mathrm{pccd0},s}}\end{bmatrix}\begin{bmatrix}\Delta u_{\mathrm{pccd},s}\\ \Delta u_{\mathrm{pccq},s}\end{bmatrix} \tag{5}$$

Considering one sampling period (T_s) for computational delay and a half-sampling period (0.5 T_s) delay related to the pulse width modulator [17], the Pade approximation is used to replace the control delay link, and its equivalent transfer function is [18]

$$G_{\mathrm{del}}(s) = e^{-1.5T_s s} \approx \frac{1 - 0.75T_s s}{1 + 0.75T_s s} \tag{6}$$

where T_s represents the sampling interval.

According to Equations (1)–(6), the small-signal mathematical model of VSC can be obtained as shown in Figure 2. The transfer function model of each link is shown in the following equation:

$$\boldsymbol{G}_{\mathrm{ays1}}(s) = \begin{bmatrix}0 & -\frac{H_{\mathrm{pll}}(s)I_{q0}}{s+H_{\mathrm{pll}}(s)U_{\mathrm{pccd0},s}}\\ 0 & \frac{H_{\mathrm{pll}}(s)I_{d0}}{s+H_{\mathrm{pll}}(s)U_{\mathrm{pccd0},s}}\end{bmatrix} \tag{7}$$

$$\boldsymbol{G}_{\mathrm{ays2}}(s) = \begin{bmatrix}0 & -\frac{H_{\mathrm{pll}}(s)v_{mq0,s}}{s+H_{\mathrm{pll}}(s)U_{\mathrm{pccd0},s}}\\ 0 & \frac{H_{\mathrm{pll}}(s)v_{md0,s}}{s+H_{\mathrm{pll}}(s)U_{\mathrm{pccd0},s}}\end{bmatrix} \tag{8}$$

$$\boldsymbol{G}_i(s) = \begin{bmatrix}H_{\mathrm{ci}}(s) & 0\\ 0 & H_{\mathrm{ci}}(s)\end{bmatrix} \tag{9}$$

$$\boldsymbol{G}_{\mathrm{de}}(s) = \begin{bmatrix}G_{\mathrm{del}}(s) & 0\\ 0 & G_{\mathrm{del}}(s)\end{bmatrix} \tag{10}$$

where $\boldsymbol{G}_{\mathrm{ays1}}(s)$ and $\boldsymbol{G}_{\mathrm{ays2}}(s)$ are correction matrices for current and modulation signal, respectively, taking into account PLL. $\boldsymbol{G}_{\mathrm{i}}(s)$ represents the current loop matrix. $\boldsymbol{G}_{\mathrm{de}}(s)$ represents the delay loop matrix.

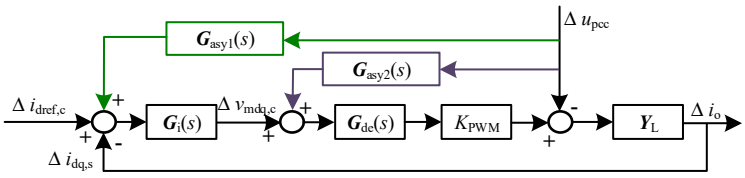

Figure 2. The small-signal model of VSC controlled in the dq frame.

According to Figure 2 and Equations (7)–(10), the impedance of the VSC with PLL working under a closed-loop condition is

$$\boldsymbol{Y}_{\mathrm{vsc}}(s) = [\boldsymbol{I}_2 + \boldsymbol{Y}_{\mathrm{L}}(s)\boldsymbol{K}_{\mathrm{PWM}}\boldsymbol{G}_{\mathrm{de}}(s)\boldsymbol{G}_{\mathrm{i}}(s)]^{-1} \cdot \boldsymbol{Y}_{\mathrm{L}}(s)[\boldsymbol{I}_2 - \boldsymbol{K}_{\mathrm{PWM}}\boldsymbol{G}_{\mathrm{de}}(s) \cdot (\boldsymbol{G}_{\mathrm{ays2}}(s) + \boldsymbol{G}_{\mathrm{i}}(s)\boldsymbol{G}_{\mathrm{ays1}}(s))] \quad (11)$$

where $\boldsymbol{I}_2$ is a second-order unit matrix.

2.2. Equivalent Model of Multi-Converter Grid-Tied System

Figure 3 shows a typical system with multi-paralleled grid-tied VSCs. According to Equation (11), the VSC is equivalent to the Norton circuit. The transmission line is represented with the equivalent grid inductance L_{g}. In the multi-converter grid-tied system, the converter section and the power grid section are considered separate subsystems [19]. The converter subsystem includes all converters, while the power grid subsystem includes transmission lines and the ideal power grid.

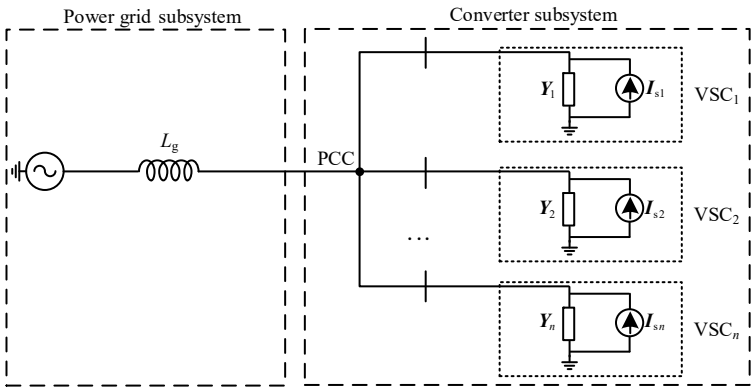

Figure 3. Parallel operation of multiple VSCs.

Furthermore, the converter subsystem can be equivalent to the form of multiple current sources and admittance in parallel as shown in Figure 3. Based on Kirchhoff's current law, its impedance model can be derived as

$$\boldsymbol{Y}(s) = \sum_{x=1}^{x=n} \boldsymbol{Y}_{\mathrm{vsc}x}(s) \quad (12)$$

The power grid subsystem only contains inductance and an ideal grid and its impedance matrix model can be accessed as

$$\boldsymbol{Z}_{\mathrm{g}}(s) = \begin{bmatrix} sL_{\mathrm{g}} & -\omega_1 L_{\mathrm{g}} \\ \omega_1 L_{\mathrm{g}} & sL_{\mathrm{g}} \end{bmatrix} \quad (13)$$

According to the relationship between the voltage and current of PCC, the return ratio matrix of the multi-converter grid-tied system can be obtained as [20].

$$\boldsymbol{L}(s) = \boldsymbol{Y}(s)\boldsymbol{Z}_{\mathrm{g}}(s) = \begin{bmatrix} L_{11} & L_{12} \\ L_{21} & L_{22} \end{bmatrix} \quad (14)$$

where L_{11}, L_{12}, L_{21}, L_{22} are the elements in the return ratio matrix $\boldsymbol{L}(s)$.

The small-signal stability of the multi-converter grid-tied system can be determined by the $\boldsymbol{L}$(s) [20].

3. Stability Analysis and Improvement in the Multi-Converter Grid-Tied System

3.1. Stability Analysis of the Multi-Converter Grid-Tied System

GNC [21,22] is the traditional method to analyze the stability of the multi-converter grid-tied system. If the Nyquist curves for the eigenvalues of $\boldsymbol{L}(s)$ do not enclose the (−1, j0) point, the system is stable. However, this method requires the complex eigenvalue decomposition of $\boldsymbol{L}(s)$, which makes this method inefficient and impractical.

To determine the system stability, it is not necessary to obtain the exact eigenvalues of the $\boldsymbol{L}(s)$. Instead, it is sufficient to assess the rough trajectory range. Therefore, the Gerschgorin disc theorem can be used to estimate the position of $\boldsymbol{L}(s)$ eigenvalues, which can simplify the judgment of system stability. Gerschgorin disc theorem [23]:

Let $\boldsymbol{A} = (a_{ij}) \in C^{n \times n}$, where a_{ij} represents the element in the i^{th} row and j^{th} column of matrix $\boldsymbol{A}$, and C represents the set of complex numbers. Gerschgorin disc is a circle with a_{ii} as its center and the sum of the modulus values of non-diagonal elements as its radius.

According to the Gerschgorin disc theorem, the eigenvalues λ_i of $\boldsymbol{L}(s)$ are located in the union of n row Gerschgorin discs O_{r} and n column Gerschgorin discs O_{c}. The accuracy of the eigenvalue estimation of $\boldsymbol{L}(s)$ can be improved by the fact that any eigenvalue of $\boldsymbol{L}(s)$ is located at the part $T(\boldsymbol{L})$ intersecting the set of O_{r} and O_{c}:

$$T(\boldsymbol{L}) = O_{\text{r}} \cap O_{\text{c}} \tag{15}$$

$$O_{\text{r}} : \bigcup_{i=1}^{2} \left\{ z \middle| |z - L_{ii}| \le R_{\text{r}i}(\boldsymbol{L}) = \sum_{\substack{j=1 \\ j \ne i}}^{2} |L_{ij}| \right\} \tag{16}$$

$$O_{\text{c}} : \bigcup_{j=1}^{2} \left\{ z \middle| |z - L_{jj}| \le R_{\text{c}j}(\boldsymbol{L}) = \sum_{\substack{i=1 \\ i \ne j}}^{2} |L_{ij}| \right\} \tag{17}$$

where $z = (x,y)$ represents a set of points in the complex plane. $R_{\text{r}i}(\boldsymbol{L})$ and $R_{\text{c}j}(\boldsymbol{A})$ represent the radius of the i^{th} row Gerschgorin disc and j^{th} column Gerschgorin disc for $\boldsymbol{L}(s)$.

According to GNC, a criterion for system stability based on the Gerschgorin disc theorem can be derived. When the trajectory of $T(\boldsymbol{L})$ does not enclose the point $(-1, \text{j}0)$, the curves of the eigenvalues of $\boldsymbol{L}(s)$ do not enclose the point $(-1, \text{j}0)$ and the system is stable. In other words, when the trajectories of the row Gerschgorin discs or the column Gerschgorin discs do not enter the region starting from the point $(-1, \text{j}0)$ and extending to the left, the system is stable. Here, the region starting from the point $(-1, \text{j}0)$ and extending to the left is defined as the forbidden zone P. The geometric condition for the stability of a multi-converter grid-tied system according to the Gerschgorin disc theorem is as follows:

$$(O_{\text{r}} \cap P) \cup (O_{\text{c}} \cap P) = \varnothing \tag{18}$$

The shortest distance from the Gerschgorin disc boundary to $[-\infty, -1]$ (pink lines) is used as the stability criterion, which is illustrated in Figure 4 [24].

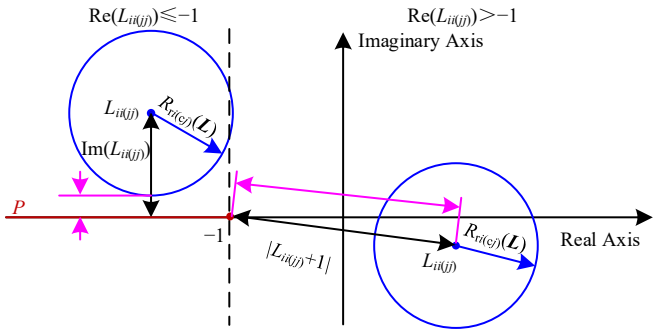

Figure 4. The geometric schematic diagram of system stability judgment conditions.

Combining Equation (18) and Figure 4, a stability evaluation function $h(f)$ for a multi-converter grid-tied system can be constructed. The expression of $h(f)$ is given by Equation (19). When the value of the lowest point M in the function $h(f)$ is greater than 0, the trajectories of the Gerschgorin discs do not enter the forbidden zone and the system is stable.

$$h(f) = \max(h_{\mathrm{r}}(f), h_{\mathrm{c}}(f)) \tag{19}$$

where

$$h_{\mathrm{r}}(f) = \begin{cases} \min(|\mathrm{Im}(L_{ii})| - R_{\mathrm{r}i}(\boldsymbol{L})), \mathrm{Re}(L_{ii}) \le -1 \\ \min(|L_{ii}+1| - R_{\mathrm{r}i}(\boldsymbol{L})), \mathrm{Re}(L_{ii}) > -1 \end{cases} \tag{20}$$

$$h_{\mathrm{c}}(f) = \begin{cases} \min(|\mathrm{Im}(L_{jj})| - R_{\mathrm{c}j}(\boldsymbol{L})), \mathrm{Re}(L_{jj}) \le -1 \\ \min(|L_{jj}+1| - R_{\mathrm{c}j}(\boldsymbol{L}), \mathrm{Re}(L_{jj}) > -1 \end{cases} \tag{21}$$

According to GNC, when the system is unstable, the farther the intersection point of the Nyquist curve of the $\boldsymbol{L}$(s) with the real axis is away from the point (−1, j0), the worse the system stability is.

$h(f)$ only considers the shortest distance from the boundary of the Gerschgorin discs to the range $[-\infty, -1]$ when $\mathrm{Re}(L_{ii(jj)}) \le -1$, without considering the distance between the fastest intersection of the Gerschgorin disc with the real axis and the point (−1, j0). Figure 5 shows that the Gerschgorin discs correspond to the lowest points M of the $h(f)$ function under different parameters. The function value M_2 under parameter 2 is greater than M_1 under parameter 1. However, the intersection point between the Gerschgorin disc and the real axis is farther from (−1, j0) under parameter 2 due to the change in the Gerschgorin disc's radius after parameter optimization, and the system stability is worse. In this scenario, the theoretical direction of parameter optimization is opposite to the actual correction direction when performing subsequent parameter sensitivity analysis on the system.

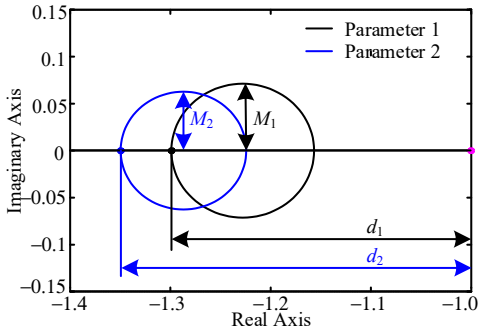

Figure 5. Scenarios of misjudgment in the stability evaluation function $h(f)$.

Based on the existing stability evaluation function, this article incorporates the distance between the intersection point and (−1, j0) when the Gerschgorin discs intersect with the real axis and $\mathrm{Re}(L_{ii(jj)}) \le -1$, as illustrated by the green double arrow line in Figure 6.

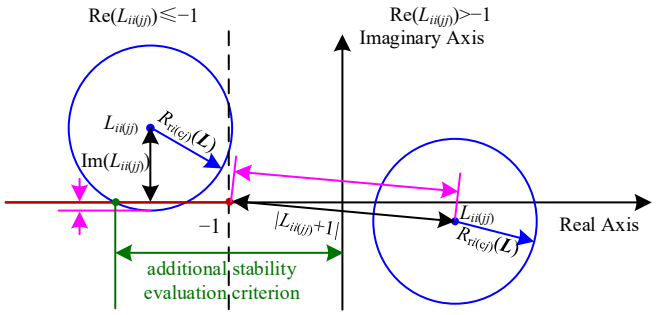

Figure 6. The geometric schematic diagram of system stability for new judgment condition.

Combining the geometric conditions for system stability defined by Equation (18) and the proposed stability evaluation criterion introduced in Figure 6, a more comprehensive stability evaluation function for the multi-converter grid-tied system can be formulated as follows.

$$g(f) = \max(g_{\mathrm{r}}(f), g_{\mathrm{c}}(f)) \tag{22}$$

where

$$g_{\mathrm{r}}(f) = \begin{cases} \min[|\mathrm{Im}(L_{ii})| - R_{\mathrm{r}i}(\boldsymbol{L}), \mathrm{Re}(L_{ii}) + 1 - \sqrt{R_{\mathrm{r}i}(\boldsymbol{L})^2 - |\mathrm{Im}(L_{ii})|^2}],\ \mathrm{Re}(L_{ii}) \le -1 \& [|\mathrm{Im}(L_{ii})| - R_{\mathrm{r}i}(\boldsymbol{L}) \le 0] \\ \min[|\mathrm{Im}(L_{ii})| - R_{\mathrm{r}i}(\boldsymbol{L})],\ \mathrm{Re}(L_{ii}) \le -1 \& [|\mathrm{Im}(L_{ii})| - R_{\mathrm{r}i}(\boldsymbol{L}) > 0] \\ \min[|L_{ii} + 1| - R_{\mathrm{r}i}(\boldsymbol{L})]\ , \mathrm{Re}(L_{ii}) > -1 \end{cases} \tag{23}$$

$$g_{\mathrm{c}}(f) = \begin{cases} \min[\left|\mathrm{Im}(L_{jj})\right| - R_{\mathrm{c}j}(\boldsymbol{L}), \mathrm{Re}(L_{jj}) + 1 - \sqrt{R_{\mathrm{c}j}(\boldsymbol{L})^2 - \left|\mathrm{Im}(L_{jj})\right|^2}],\ \mathrm{Re}(L_{ii}) \le -1 \& [\left|\mathrm{Im}(L_{jj})\right| - R_{\mathrm{c}j}(\boldsymbol{L}) \le 0] \\ \min[\left|\mathrm{Im}(L_{jj})\right| - R_{\mathrm{c}j}(\boldsymbol{L})],\ \mathrm{Re}(L_{jj}) \le -1 \& [\left|\mathrm{Im}(L_{jj})\right| - R_{\mathrm{c}j}(\boldsymbol{L}) > 0] \\ \min[\left|L_{jj} + 1\right| - R_{\mathrm{c}j}(\boldsymbol{L})],\ \mathrm{Re}(L_{jj}) > -1 \end{cases} \tag{24}$$

The rules for determining system stability based on the stability evaluation function are illustrated in Figure 7. When the function value of the lowest point M of $g(f)$ is greater than 0, it means that the trajectory of the Gerschgorin discs does not enter the forbidden zone, and the system is stable. Otherwise, the system is unstable. Thus, M can be used to quantitatively characterize the stability of a system, in which a larger function value for M implies better system stability.

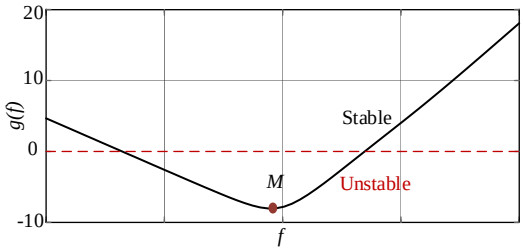

Figure 7. Stability evaluation function for the multi-converter grid-tied system.

3.2. Parameter Optimization

The $g(f)$ function derived in Section 3.1 is used to evaluate the stability of the multi-converter grid-tied system. When the system is unstable, researching the influence of VSCs control parameters on system stability is vital. Parameter optimization based on the identification of the stability-weakest parameters is essential for improving system stability, which is performed based on the $g(f)$ function in this section.

Let $g(f) = g(f, \boldsymbol{x})$, where $\boldsymbol{x} = \{x_1, x_2, \ldots, x_n\}$ is the set of any adjustable parameter in the multi-converter grid-tied system. As shown in Equation (22), $g(f, \boldsymbol{x})$ is a piecewise function about $\boldsymbol{x}$. When the adjustable parameter changes slightly, the $g(f)$ function can be linearized around the initial values $\boldsymbol{x}_0 = \{x_{10}, x_{20}, \ldots, x_{n0}\}$, according to the Taylor expansion:

$$\begin{cases} g(f, \boldsymbol{x}) \approx g(f, \boldsymbol{x}_0) + \mu_{x10}(f)(x_1 - x_{10}) + \mu_{x12}(f)(x_2 - x_{20}) + \ldots + \mu_{xn0}(f)(x_n - x_{n0}) \\ \mu_{xn0}(f) = \frac{\partial g(f, \boldsymbol{x})}{\partial x_n} | \boldsymbol{x} = \boldsymbol{x}_0 \end{cases} \tag{25}$$

Define $\mu_{xi0}(f)$ as the sensitivity function of the adjustable parameter x_i at the value of x_{i0}.

According to Equation (22) and Figure 7, it can be observed that when the function value of the lowest point M of $g(f)$ is less than 0, the multi-converter grid-tied system is unstable. The objective of parameter optimization under this criterion is to modify the parameter $\boldsymbol{x}$ to ensure that the function value of M is greater than 0, thereby achieving system stability.

Thus, the following parameter optimization criteria are applied to any adjustable parameter $\boldsymbol{x}$:

(1) At a specific frequency, if the sensitivity function value $\mu_{xi0}(f) > 0$ for parameter x_i, the parameter x_i needs to be increased to increase the value of function $g(f)$ according to Equation (25). Conversely, if $\mu_{xi0}(f) < 0$, the parameter x_i needs to be decreased.

(2) If $|\mu_{xi0}(f)| > |\mu_{xj0}(f)|$, the variation of parameter x_i has a greater impact on system stability at this frequency. So the parameters with large absolute sensitivity values are defined as stability-weakest parameters. When system stability cannot be satisfied by optimizing a single parameter, parameter optimization can be performed by combining stability-weakest parameters.

(3) Perform parameter optimization for m ($m \geq 1$) parameters. Assume that the sensitivity values of these parameters have the same sign and equal optimization magnitude. Then, according to Equation (25), the modified values for parameter $x_{i\,|\,i=1,2,\ldots,m}$, to ensure that the function value of M is greater than 0, are given as:

$$x_i = x_{i0} + \frac{-g(f, \boldsymbol{x}_0)}{\sum_{i=1}^{m} \mu_{xi0}(f)} \tag{26}$$

The process of system parameter optimization based on parameter sensitivity analysis in Figure 8 is as follows.

Step1: Firstly, the return ratio matrix $\boldsymbol{L}(s)$ of the multi-converter grid-tied system is obtained.
Step2: Then, the stability evaluation function $g(f)$ of the system is constructed according to the Gerschgorin disc theorem and GNC to determine the system stability.
Step3: If the system is unstable, get the function and the frequency value of the M, and calculate the parameter sensitivity of each parameter.
Step4: Finally, the stability-weakest parameters are identified. The parameter optimization values are calculated according to the parameter optimization criteria.

The parameter optimization value is calculated by several iterations until the function value of M is above zero, which means the system satisfies the requirement of stability.

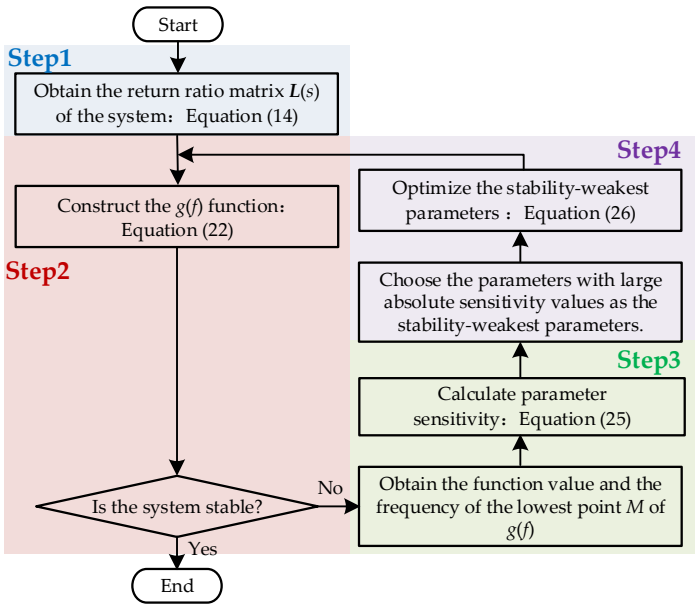

Figure 8. Flowchart of parameter optimization for a multi-converter grid-tied system.

4. Analysis and Simulation Verification

4.1. Optimization of One Parameter

To verify the effectiveness of the proposed method for analyzing and improving the stability of the multi-converter grid-tied system, a three-VSC system is built as shown in Figure 3. Differentiated control parameters for VSCs are employed to emphasize the distinctions between different VSCs. The system under the grid parameters and control parameters of VSCs presented in Table A1 (Appendix A) is defined as system A.

Obtaining the return ratio matrix $\boldsymbol{L}$(s) of system A, the $h(f)$ and $g(f)$ functions are constructed according to Equations (19) and (22) and plotted in Figure 9a,b, respectively. From Figure 9, it can be observed that the function values of the lowest points M for both $h(f)$ and $g(f)$ are less than 0, and system A is unstable.

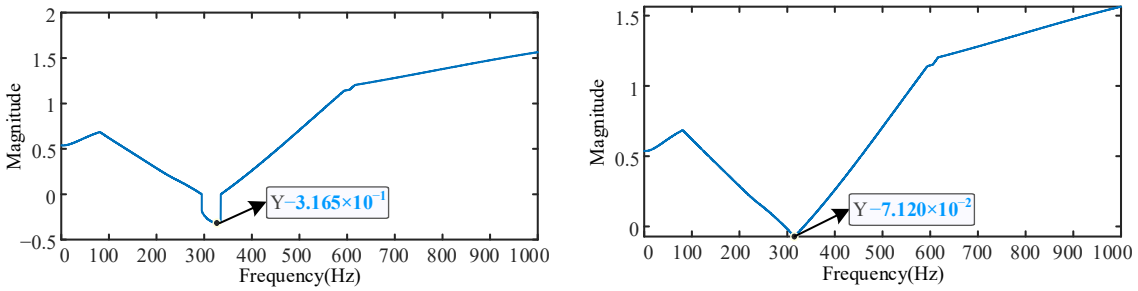

(**a**) (**b**)

Figure 9. Stability evaluation function of system A under the initial parameters: (**a**) $h(f)$ function; (**b**) $g(f)$ function.

When system A is unstable, parameter sensitivity analysis is required to identify the stability-weakest parameters according to Equation (25). Existing research has shown that the proportional parameters of the current loop [25] and PLL [26] in VSC have a greater impact on system stability compared to the integral parameters. Therefore, this article focuses on analyzing the impact of the proportional parameters in different VSCs on system A stability. The sensitivity results for each parameter are presented in Table 1.

Table 1. Parameter sensitivity results of system A under initial condition.

Parameter	k_{ip1}	k_{ip2}	k_{ip3}	k_{pllp1}	k_{pllp2}	k_{pllp3}
parameter sensitivity of $h(f)$	141.8	15.47	3.015	1.378×10^{-1}	7.190×10^{-2}	5.430×10^{-2}
parameter sensitivity of $g(f)$	−915.7	−66.22	−66.29	-1.643×10^{-1}	-3.334×10^{-1}	-3.306×10^{-1}

The sign of parameter sensitivity determines the direction of parameter optimization, according to parameter sensitivity optimization criterion 1. The sensitivity calculation results for the $h(f)$ and $g(f)$ functions exhibit opposite signs: positive values of parameter sensitivity for $h(f)$ indicate an increase in the parameter, while negative values of parameter sensitivity for $g(f)$ suggest a decrease in the parameter. The analytical conclusions of the traditional method and the method proposed in this paper are contradictory.

The distance between the Nyquist curves of $\boldsymbol{L}(s)$ and the $(-1, j0)$ point can be used to evaluate the stability of system A. It can verify which method's parameter optimization direction is correct. Taking the parameter k_{ip1} as an example, Figure 10 illustrates the changes in the Nyquist curves of system A. Figure 10 only displays the curves of the eigenvalues that have a substantial impact on the system. When k_{ip1} increases, the Nyquist curves of system A move away from the $(-1, j0)$ point, and system A stability deteriorates. Meanwhile, when k_{ip1} decreases, the Nyquist curves move closer to the $(-1, j0)$ point, and system A stability is improved. There is a misjudgment about the optimization direction of the $h(f)$ function. It theoretically demonstrates that the method proposed in this paper can overcome the defect of traditional methods caused by the misjudgment of parameter optimization direction due to the change in the Gerschgorin disc's radius after parameter optimization.

Following the second rule of parameter optimization, parameters with larger absolute sensitivity values have a greater impact on the system stability. By sorting the parameters based on the absolute values of their parameter sensitivities, the influence of each VSC parameter on system stability can be determined as follows: $k_{ip1} > k_{ip3} > k_{ip2} > k_{pllp2} > k_{pllp3} > k_{pllp1}$.

When parameters change, the change degree of Nyquist curves can be used to judge the influence of parameters on system A stability, to verify the correctness of parameter sensitivity analysis. Figure 11 illustrates the Nyquist curves of system A when one control parameter of VSC is altered -5.000×10^{-4} while keeping other parameters constant. It depicts that when all parameters are reduced, the Nyquist curves of system A approach the point $(-1, j0)$, and the system stability is improved. Furthermore, according to the change degree of Nyquist curves, parameters are sorted as follows: $k_{ip1} > k_{ip3} > k_{ip2} > k_{pllp2} > k_{pllp3} > k_{pllp1}$. This validation confirms the correctness and effectiveness of the proposed parameter sensitivity analysis method.

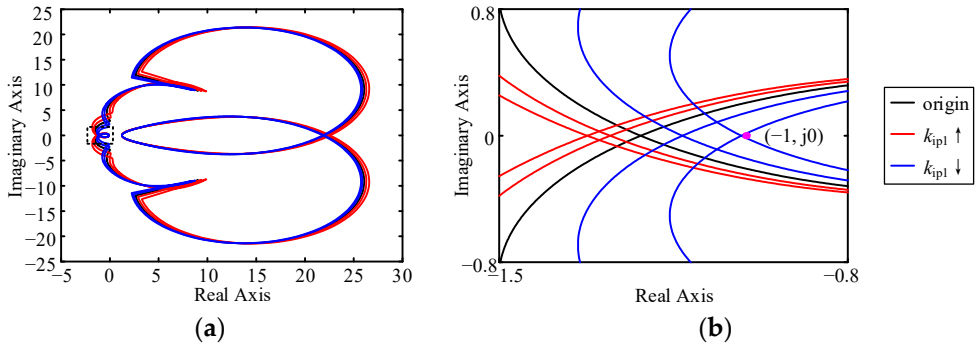

Figure 10. Nyquist curves of system A with different k_{ip1} parameters: (**a**) integrated graph; (**b**) partial enlargement (**a**).

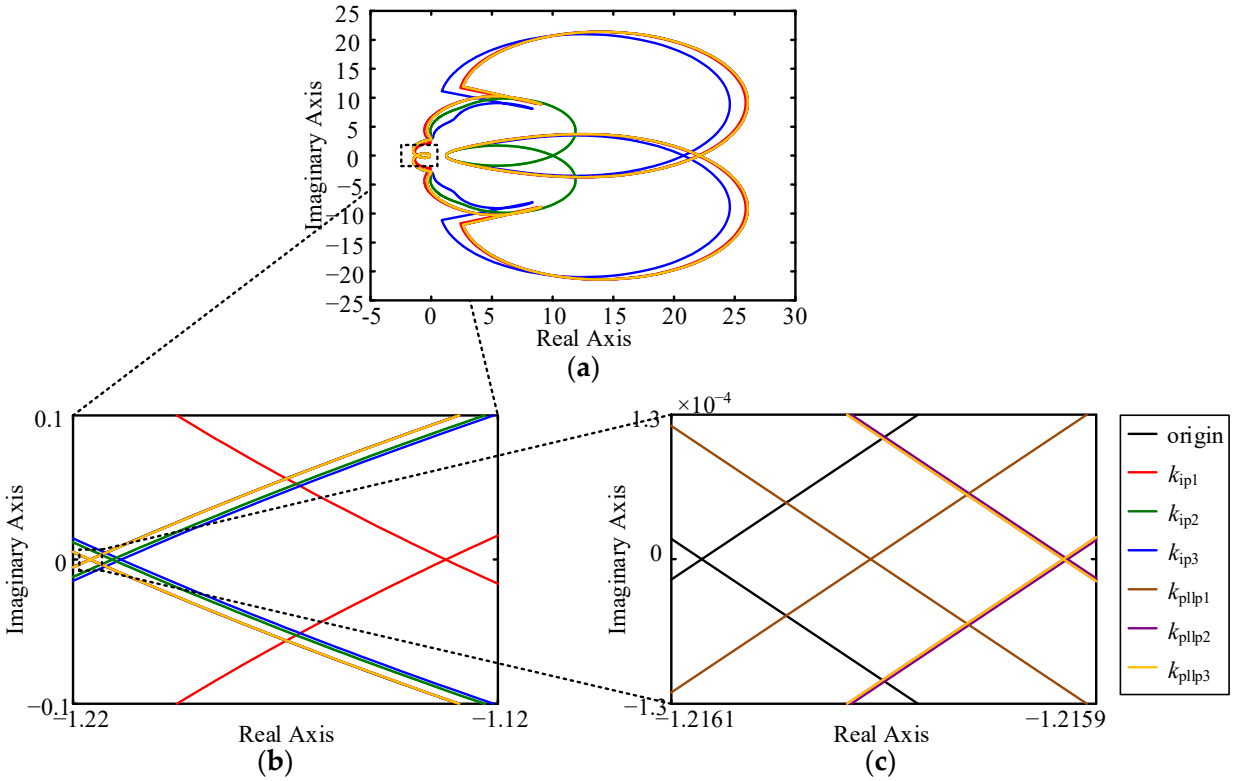

Figure 11. Nyquist curves of system A with different VSC control parameters: (**a**) integrated graph; (**b**) partial enlargement of (**a**); (**c**) partial enlargement of (**b**).

To improve the stability of system A, parameter optimization is performed on the stability-weakest parameter based on the third criterion of the parameter optimization rules. From Table 1, the absolute sensitivity value of the k_{ip1} parameter is significantly larger than that of other parameters; thereby, k_{ip1} is the stability-weakest parameter. Combining Equation (26) and Figure 9b, the calculation yields a new value for k_{ip1} as 1.800×10^{-3}. The return ratio matrix of the new system is re-obtained to construct the $g(f)$ function, as shown in Figure 12. It can be seen that the function value of the lowest point for the $g(f)$ function is -2.682×10^{-1}, which is larger than that of the previous $g(f)$ function, but still less than 0. Therefore, parameter optimization needs to be continued.

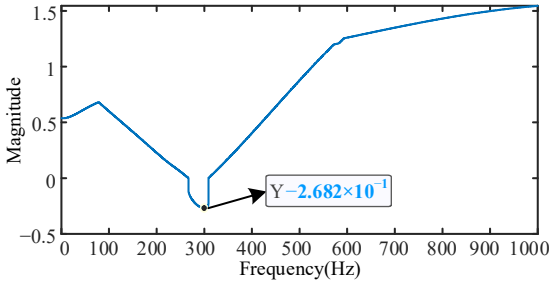

Figure 12. $g(f)$ function after the first parameter optimization ($k_{ip1} = 1.800 \times 10^{-3}$).

Based on the flowchart shown in Figure 8, the parameter optimization value of k_{ip1} is finally calculated as 4.600×10^{-4}. Figure 13 shows system A's function $g(f)$ under final parameter optimization, and its function value at the lowest point is 4.700×10^{-3}, which indicates the system is stable.

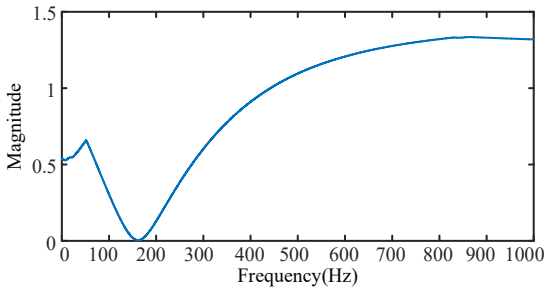

Figure 13. $g(f)$ function of system A under final parameter optimization ($k_{ip1} = 4.600 \times 10^{-4}$).

To verify the theoretical analysis results mentioned above, the time-domain simulations based on MATLAB/Simulink are performed. Figure 14 shows the PCC voltage before and after modifying different control parameters of the VSCs while keeping other parameters constant. Figure 14a presents the waveform of PCC voltage during the optimization of k_{ip1}. System A is oscillated for 2 s. At 2 s, k_{ip1} is optimized to 1.800×10^{-3}, reducing system A oscillations but still being unstable. At 2.2 s, k_{ip1} is further optimized to 4.600×10^{-4}, and system A regains stability. Parameter optimization of weak stability parameters can effectively improve the stability of the system.

Furthermore, Figure 14b–f shows that as k_{ip2}, k_{ip3}, k_{pllp1}, k_{pllp2}, and k_{pllp3} decrease, the oscillation of the PCC voltage is significantly improved. This is consistent with the sign results of parameter sensitivity calculated in Table 1.

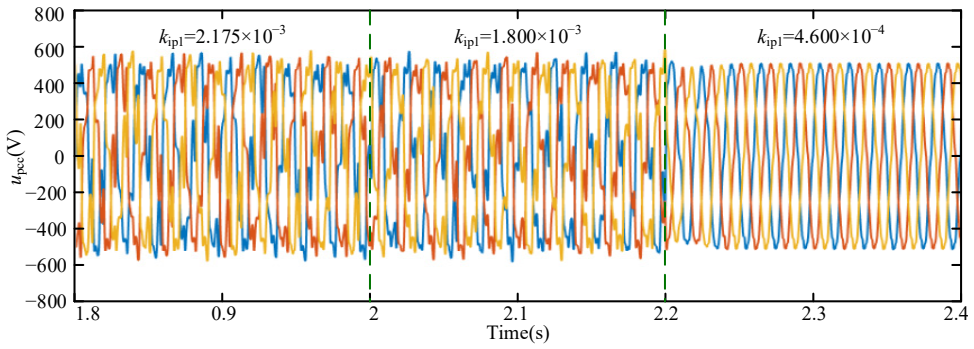

(**a**)

Figure 14. *Cont.*

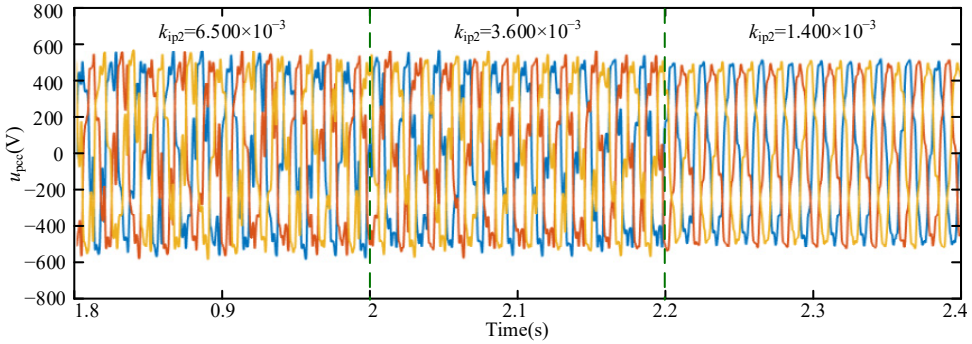

(**b**)

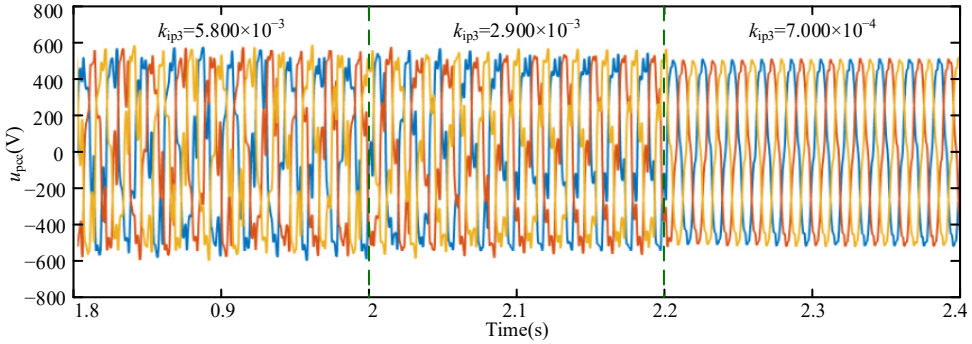

(**c**)

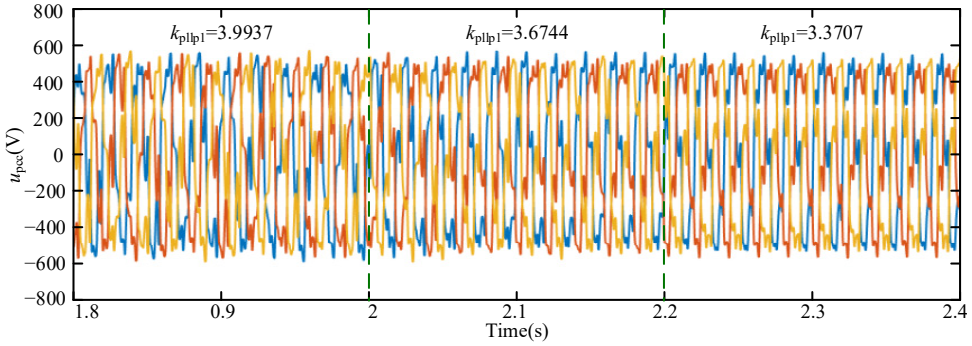

(**d**)

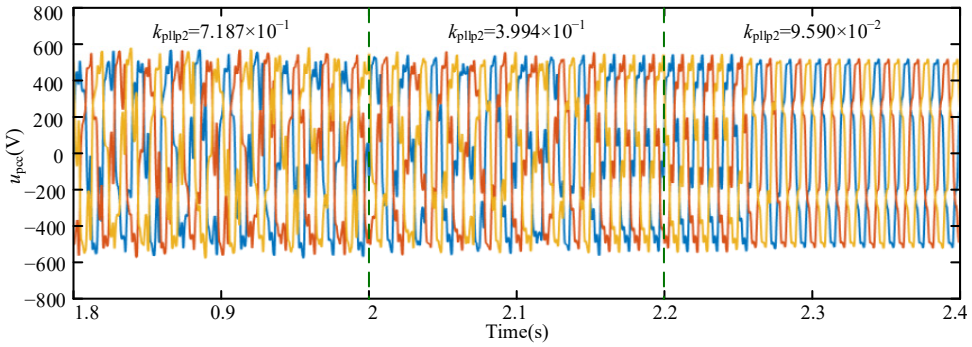

(**e**)

Figure 14. *Cont.*

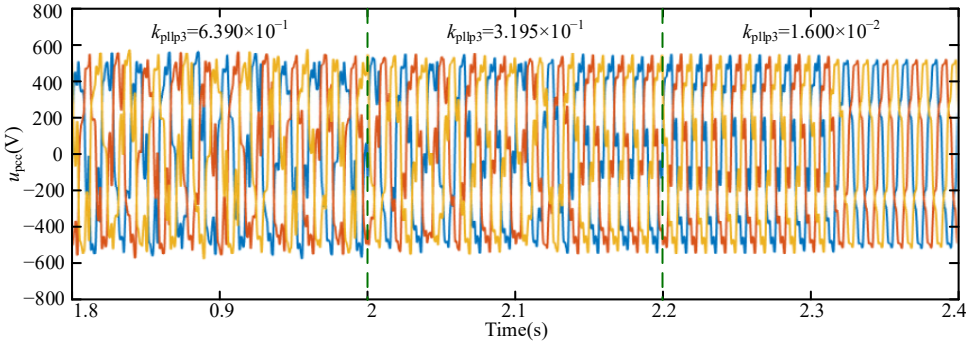

Figure 14. PCC voltage waveforms before and after VSC parameter modification: (**a**) k_{ip1} parameter modification; (**b**) k_{ip2} parameter modification; (**c**) k_{ip3} parameter modification; (**d**) k_{pllp1} parameter modification; (**e**) k_{pllp2} parameter modification; (**f**) k_{pllp3} parameter modification.

Table 2 summarizes the harmonic content of the PCC voltage before and after the modification of VSC parameters, as illustrated in Figure 14. From Table 2, it can be observed that k_{ip1} has the smallest change in parameter value, but the largest change in harmonic content. Minimally changing the stability-weakest parameters can effectively improve the stability of the system.

Table 2. The harmonic content of PCC voltage before and after VSC control parameter modification.

	Value	**Value**	**Value**	**Variation**
k_{ip1} Parameter	2.175×10^{-3}	1.800×10^{-3}	4.600×10^{-4}	1.715×10^{-3}
Harmonic Content	32.81%	30.68%	5.050%	27.76%
k_{ip2} Parameter	6.500×10^{-3}	3.600×10^{-3}	1.400×10^{-3}	5.100×10^{-3}
Harmonic Content	32.81%	28.03%	12.22%	20.59%
k_{ip3} Parameter	5.800×10^{-3}	2.900×10^{-3}	7.000×10^{-4}	5.1000×10^{-3}
Harmonic Content	32.81%	27.84%	8.060%	24.75%
k_{pllp1} Parameter	3.994	3.674	3.371	0.6230
Harmonic Content	32.81%	28.78%	27.99%	4.820%
k_{pllp2} Parameter	0.7189	0.3994	9.590×10^{-2}	0.6230
Harmonic Content	32.81%	24.98%	12.22%	20.59%
k_{pllp3} Parameter	0.6390	0.3195	1.600×10^{-2}	0.6230
Harmonic Content	32.81%	24.76%	14.02%	18.79%

The parameter change of k_{ip2} and k_{ip3} is the same, but the change in harmonic content for k_{ip3} (24.75%) is greater than that for k_{ip2} (20.59%). It indicates that k_{ip3} has a greater impact on system A stability compared to k_{ip2}. The corresponding change in harmonic content for $k_{pllpi\,|\,i=1,\,2,\,3}$ is smaller than that for $k_{ipi\,|\,i=1,\,2,\,3}$ when the variation of k_{pllpi} is larger than that for k_{ipi}. Thus, k_{pllpi} has a smaller impact on system A stability compared to k_{ipi}. The remaining parameters are analyzed using the same method. The ranking of the control parameters for VSCs based on their impact on system A stability is as follows: $k_{ip1} > k_{ip3} > k_{ip2} > k_{pllp2} > k_{pllp3} > k_{pllp1}$, which is consistent with the theoretical analysis results.

The above simulation results verify the correctness of the proposed method in this paper. This method can intuitively and quantitatively analyze the impact of parameters on system stability, and optimize the stability-weakest parameter to effectively improve system stability.

4.2. Optimization of Multiple Parameters

When the system stability cannot be satisfied by the optimization of a single parameter, it is necessary to promote system stability through joint adjustment of multiple parameters. To verify the adaptability of the method proposed in this paper to this situation, the control parameters of the VSCs are modified. The control parameters are listed in Table A2. Define the system as system B.

According to Equation (22), the $g(f)$ function is constructed by obtaining the $\boldsymbol{L}(s)$ for the multi-converter grid-tied system, and is plotted in Figure 15. Figure 15 shows the minimum value of the $g(f)$ is -6.446×10^{-1} less than 0 at point M, indicating the system is unstable.

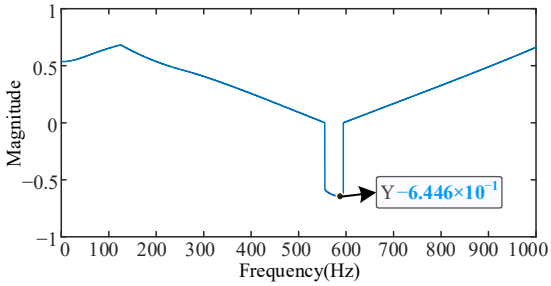

Figure 15. Stability evaluation function of system B under initial parameters (in Table A2).

The parameter sensitivity of each VSC parameter under the $g(f)$ at the point M is calculated, respectively, according to Equation (25) and presented in Table 3. Sorting parameters based on the magnitude of their sensitivities, the influence of each VSC parameter on system stability is as follows: $k_{ip2} > k_{ip3} > k_{ip1} > k_{pllp2} > k_{pllp3} > k_{pllp1}$.

Table 3. Parameter sensitivity of system B under initial parameters (in Table A2).

Parameter	k_{ip1}	k_{ip2}	k_{ip3}	k_{pllp1}	k_{pllp2}	k_{pllp3}
parameter sensitivity	2.907	−107.8	−79.93	−0.2990	−0.3447	−0.3247

The same analysis method as in Figure 11 is used to verify the correctness of the parameter sensitivity analysis method. The variation of k_{ip1} is 5.000×10^{-4} and the variation of other parameters is -5.000×10^{-4}. Figure 16 depicts that increasing k_{ip1} and decreasing other parameters both bring the Nyquist curves of system B closer to the (−1, j0) point, and system B stability is improved. According to the degree to which changing parameters makes the Nyquist curves approach (−1, j0), the ranking of parameters is as follows: $k_{ip2} > k_{ip3} > k_{ip1} > k_{pllp2} > k_{pllp3} > k_{pllp1}$. This ranking aligns with the result of the parameter sensitivity analysis method.

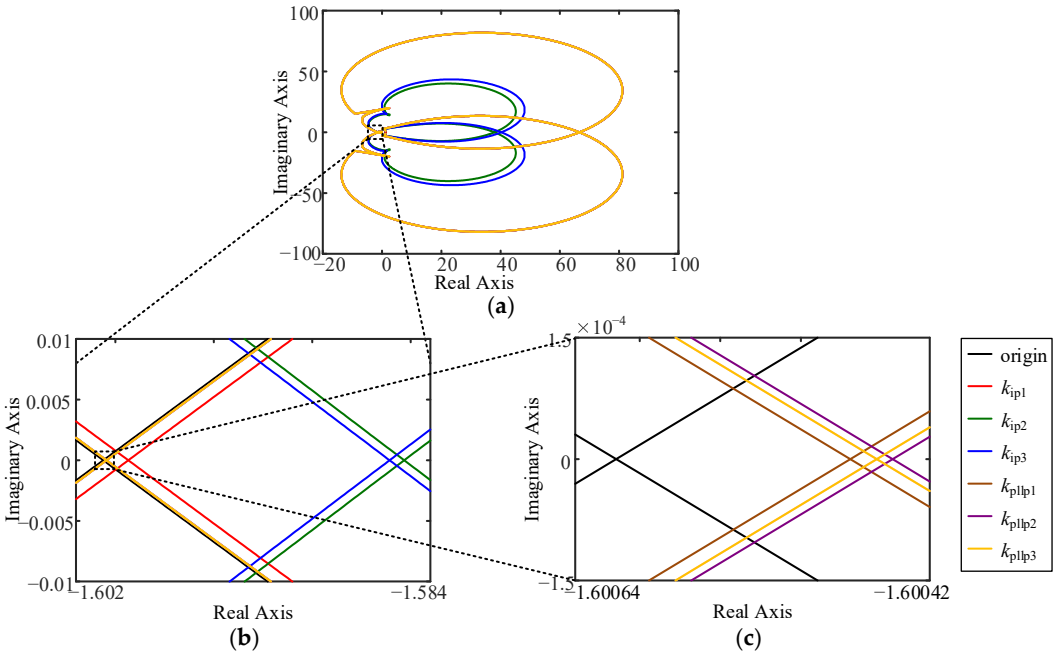

Figure 16. Nyquist curves of system B with different VSC control parameters: (**a**) integrated graph; (**b**) partial enlargement of (**a**); (**c**) partial enlargement of (**b**).

The parameter optimization is performed to stabilize the multi-converter grid-tied system. As shown in Table 3, the absolute values of parameter sensitivity for k_{ip2} and k_{ip3} are much larger than those for other parameters, so they are identified as the stability-weakest parameters. Following the flowchart shown in Figure 8 the optimization values of k_{ip2} and k_{ip3} are iteratively calculated. The calculation of k_{ip2} and k_{ip3} is 8.800×10^{-4}. At this point, the $g(f)$ is illustrated in Figure 17, which exhibits a minimum value of 4.100×10^{-3}, indicating the system is stable.

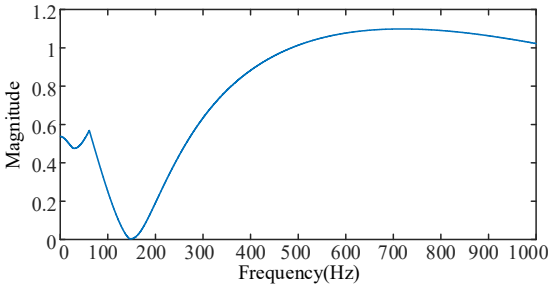

Figure 17. $g(f)$ function of system B under final parameter optimization ($k_{ip2} = 8.8000 \times 10^{-4}$, $k_{ip3} = 8.8000 \times 10^{-4}$).

The waveforms of the PCC voltage before and after the optimization of k_{ip2} and k_{ip3} are illustrated in Figure 18. Figure 18a shows that the PCC voltage oscillates before parameter optimization. After optimizing k_{ip2} and k_{ip3} from 6.600×10^{-3} to 8.800×10^{-4}, system B is stable as shown in Figure 18b. While only optimizing k_{ip2} at the same magnitude, which has the highest absolute sensitivity, the PCC voltage continues to oscillate as shown in Figure 19a. Continuing to reduce k_{ip2}, the PCC voltage is still unstable as shown in Figure 19b. Reducing k_{ip2} can significantly improve the PCC voltage oscillation, but it cannot achieve system stability.

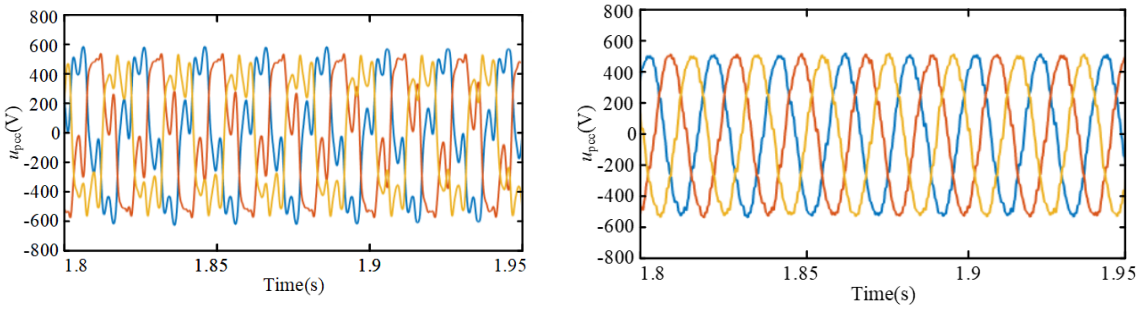

(**a**) (**b**)

Figure 18. PCC voltage waveforms before and after VSC parameter modification: (**a**) $k_{ip2} = 6.600 \times 10^{-3}$, $k_{ip3} = 6.600 \times 10^{-3}$; (**b**) $k_{ip2} = 8.800 \times 10^{-4}$, $k_{ip3} = 8.800 \times 10^{-4}$.

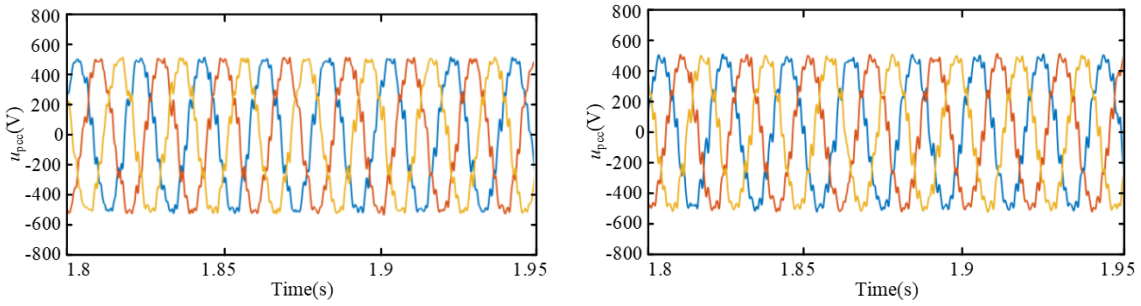

(**a**) (**b**)

Figure 19. PCC voltage waveforms after only optimizing the k_{ip2} parameter: (**a**) $k_{ip2} = 8.800 \times 10^{-4}$; (**b**) $k_{ip2} = 2.500 \times 10^{-4}$.

Therefore, when single-parameter optimization is always unable to meet the requirements of system stability, the system can be stabilized by optimizing multiple parameters in combination.

4.3. Real-Time Simulation-Based Validation

To further validate the effectiveness of the proposed parameter optimization method, a multi-converter grid-tied system model is constructed on the RT-LAB platform. Figure 20 shows the details of the RT-LAB platform. It contains a Canadian OPAL-RTLAB real-time simulation machine OP5700 (a Xilinx Virtex-7 FPGA with 32 Intel Xeon processing cores) and a host PC, which is utilized for the real-time emulation of a multi-converter grid-tied system. The waveforms are measured through the I/O ports of RT-LAB. The host PC and LeCroy oscilloscope save the real-time simulation-based results. The parameters of the grid and VSCs are the same as in Tables A1 and A2.

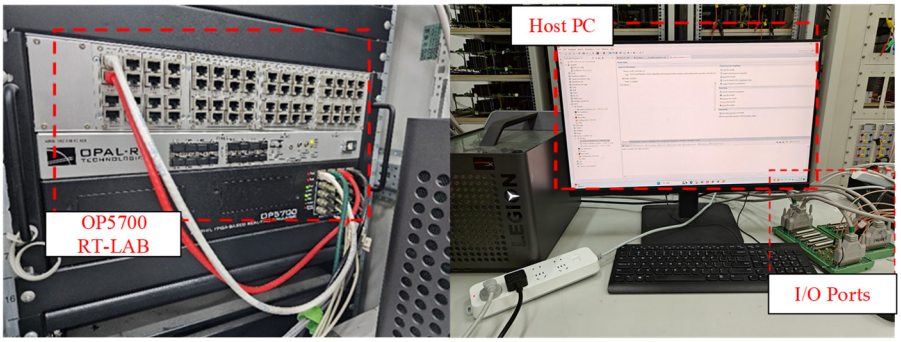

Figure 20. Detailed implementation of the RT-LAB platform.

Figure 21 illustrates the PCC voltage before and after modifying the stability-weakest parameter K_{ip1} of system A. Before optimization, system A is unstable as shown in Figure 21a. According to the previous theoretical analysis, the parameter optimization value of K_{ip1} is 4.6×10^{-4}. After optimizing k_{ip1} from 2.175×10^{-3} to 4.600×10^{-4}, system A is stable as shown in Figure 21b. Figure 22 illustrates the PCC voltage before and after optimization of the stability-weakest parameters K_{ip2} and K_{ip3} in system B. Figure 22a shows the PCC voltage waveform of system B before parameter optimization. It can be seen that system B oscillates and is unstable. According to the previous theoretical analysis, the parameter optimization values of K_{ip2} and K_{ip3} are 8.800×10^{-4}. After optimizing k_{ip2} and k_{ip3} from 6.600×10^{-3} to 8.800×10^{-4}, system B is stable as shown in Figure 22b. The real-time simulation-based results are in agreement with the theoretical analysis and simulation results in Figures 14a and 18. The real-time simulation-based results verify the correctness of the proposed method. The proposed parameter optimization method can effectively improve the stability of the multi-converter grid-connected system.

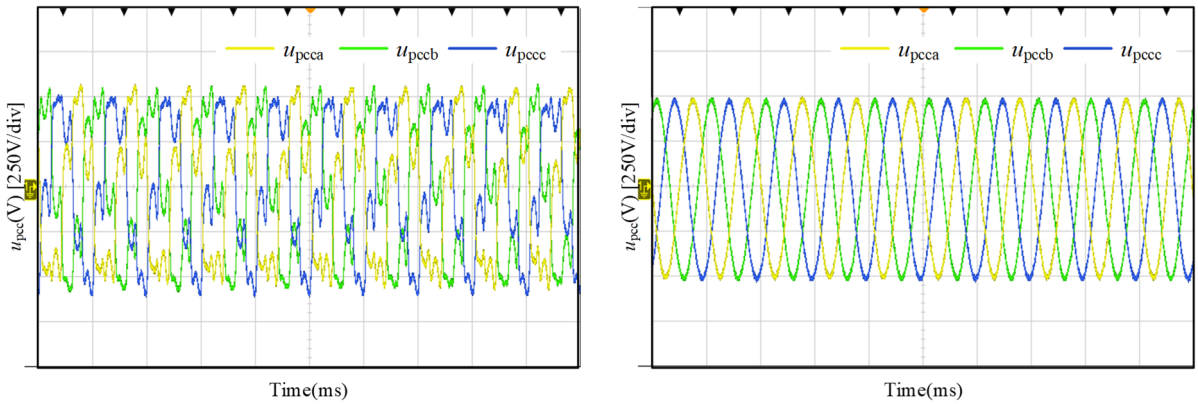

Figure 21. Real-time simulation-based results of system A before and after VSC parameter modification: (**a**) $k_{ip1} = 2.175 \times 10^{-3}$; (**b**) $k_{ip1} = 4.600 \times 10^{-4}$.

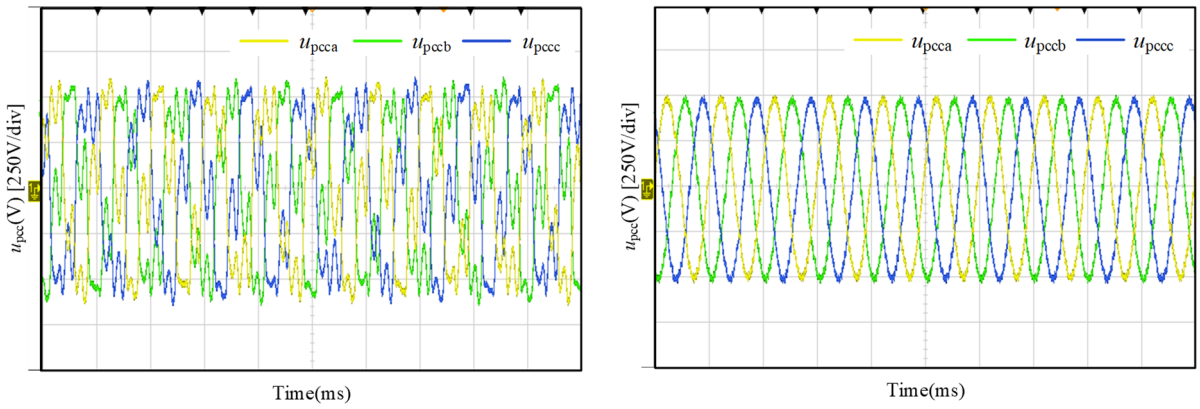

Figure 22. Real-time simulation-based results of system B before and after VSC parameter modification: (**a**) $k_{ip2} = 6.600 \times 10^{-3}$, $k_{ip3} = 6.600 \times 10^{-3}$; (**b**) $k_{ip2} = 8.800 \times 10^{-4}$, $k_{ip3} = 8.800 \times 10^{-4}$.

5. Conclusions

For the small-signal instability caused by the multi-VSCs connected to the grid, existing methods can only identify stability-weakest parameters without calculating the accurate parameter optimization values. To address this issue, this article proposes a parameter optimization to improve the stability of a multi-converter grid-tied system. The method can accurately identify the stability-weakest parameters and calculate the corresponding parameter optimization values. Specifically, the conclusions and contributions are summarized as follows:

(1) An improved stability evaluation function is constructed by considering the distance between the intersection point and (−1, j0) when the Gerschgorin discs intersect with the real axis and $\mathrm{Re}(L_{ii(jj)}) \leq -1$. This method overcomes the misjudgment of parameter sensitivity correction direction when the radius of the Gerschgorin disc changes due to the changes in VSC control parameters.

(2) In the multi-converter grid-tied system, the contribution of control parameters in each VSC to the system stability varies. The proposed method can quantitatively analyze the influence of VSC control parameters on the stability of the multi-converter grid-tied system, and identify the parameters with large absolute sensitivity as the stability weak parameters.

(3) Based on stability evaluation functions and parameter sensitivity analysis, an iterative calculations-based parameter optimization is developed. In the iterative calculations, one or multiple stability-weakest parameters can be rolling-optimized based on the quantitative results of the stability evaluation function. Theoretical analysis and simulation verify the correctness and feasibility of this approach.

Author Contributions: Conceptualization, B.C., Q.S. and P.J.; methodology, B.C. and Q.S.; software, Q.S.; validation, B.C., Q.S. and X.Z.; formal analysis, X.Z.; investigation, X.Z.; resources, B.C., Q.S. and P.J.; data curation, B.C. and Q.S.; writing—original draft preparation, Q.S.; writing—review and editing, B.C. and X.Z.; visualization, P.J.; supervision, X.Z.; project administration, B.C; funding acquisition, B.C. All authors have read and agreed to the published version of the manuscript.

Funding: This study is supported by the Science and Technology Project of State Grid Jiangxi Electric Power Co., Ltd. (NO: 521820220006, Stability analysis and operation control technology for high proportion new energy integration into AC/DC power grids).

Institutional Review Board Statement: Not applicable.

Informed Consent Statement: Not applicable.

Data Availability Statement: Data is contained within the article.

Acknowledgments: Acknowledgments to Zhiping Wu and Yongsheng Zhang for their valuable contributions to the study reflected in this manuscript.

Conflicts of Interest: Author Bo Chen was employed by the company Electric Power Research Institute of State Grid Jiangxi Electric Power Co., Ltd. The remaining authors declare that the research

was conducted in the absence of any commercial or financial relationships that could be construed as a potential conflict of interest.

Appendix A

Table A1 shows the grid parameters and the control parameters of VSCs in system A.

Table A1. Parameters of system A.

Equipment	Parameter	Symbol	Value
Grid	Grid Voltage(line-to-line)	U_g	690.0 V
	Grid Inductance	L_g	1.333×10^{-4} mH
VSC_1	Filter Inductance	L_1	3.200×10^{-4} mH
	Switching Frequency	f_{s1}	10.00 kHz
	PI Controller of Current Loop	k_{ip1}, k_{ii1}	2.175×10^{-3}, 2.900×10^{-2}
	PI Controller of PLL	k_{pllp1}, k_{plli1}	3.994, 8.870×10^{-2}
VSC_2	Filter Inductance	L_2	3.200×10^{-4} mH
	Switching Frequency	f_{s2}	10.00 kHz
	PI Controller of Current Loop	k_{ip2}, k_{ii2}	6.500×10^{-3}, 2.900×10^{-2}
	PI Controller of PLL	k_{pllp2}, k_{plli2}	7.189×10^{-1}, 1.600×10^{-2}
VSC_3	Filter Inductance	L_3	3.200×10^{-4} mH
	Switching Frequency	f_{s3}	10.00 kHz
	PI Controller of Current Loop	k_{ip}, k_{ii3}	5.800×10^{-3}, 2.900×10^{-2}
	PI Controller of PLL	k_{pllp3}, k_{plli3}	6.390×10^{-1}, 1.420×10^{-2}

Table A2 shows the grid parameters and the control parameters of VSCs in system B.

Table A2. Parameters of system B.

Equipment	Parameter	Symbol	Value
Grid	Grid Voltage(line-to-line)	U_g	690.0 V
	Grid Inductance	L_g	1.333×10^{-4} mH
VSC_1	Filter Inductance	L_1	3.200×10^{-4} mH
	Switching Frequency	f_{s1}	10.00 kHz
	PI Controller of Current Loop	k_{ip1}, k_{ii1}	1.810×10^{-2}, 3.622
	PI Controller of PLL	k_{pllp1}, k_{plli1}	3.515, 0.3905
VSC_2	Filter Inductance	L_2	3.200×10^{-4} mH
	Switching Frequency	f_{s2}	10.00 kHz
	PI Controller of Current Loop	k_{ip2}, k_{ii2}	6.600×10^{-3}, 0.1449
	PI Controller of PLL	k_{pllp2}, k_{plli2}	1.198, 2.660×10^{-2}
VSC_3	Filter Inductance	L_3	3.200×10^{-4} mH
	Switching Frequency	f_{s3}	10.00 kHz
	PI Controller of Current Loop	k_{ip}, k_{ii3}	6.600×10^{-3}, 0.1449
	PI Controller of PLL	k_{pllp3}, k_{plli3}	8.786×10^{-1}, 1.950×10^{-2}

References

1. Rodriguez, S.F.; Rosales, V.R.; Gomez-Montero, O.; Rodriguez-Hernandez, O.; Salgado-Herrera, N.M.; H-Sanchez, J.; Rodriguez-Rodriguez, J.R. Real Time Simulation of Distributed Renewable Energy Access Based on Photovoltaic Energy Conversion System. In Proceedings of the 2020 IEEE Power & Energy Society General Meeting (PESGM), Montreal, QC, Canada, 2 August 2020; pp. 1–5.
2. Qazi, A.; Hussain, F.; Rahim, N.A.; Hardaker, G.; Alghazzawi, D.; Shaban, K.; Haruna, K. Towards Sustainable Energy: A Systematic Review of Renewable Energy Sources, Technologies, and Public Opinions. *IEEE Access* **2019**, *7*, 63837–63851. [CrossRef]
3. Liao, K.; Pang, B.; Yang, J.; He, Z. Output Current Quality Improvement for VSC With Capability of Compensating Voltage Harmonics. *IEEE Trans. Ind. Electron.* **2023**, *2023*, 3327548. [CrossRef]

4. Cheng, Y.; Fan, L.; Rose, J.; Huang, S.-H.; Schmall, J.; Wang, X.; Xie, X.; Shair, J.; Ramamurthy, J.R.; Modi, N.; et al. Real-World Subsynchronous Oscillation Events in Power Grids With High Penetrations of Inverter-Based Resources. *IEEE Trans. Power Syst.* **2023**, *38*, 316–330. [CrossRef]
5. Lin, J.; Li, Y.; Hu, S.; Liu, Q.; Zhang, J.; Wang, S.; Dong, L.; Ni, J. Resonance Mechanism Analysis of Large-Scale Photovoltaic Power Plant. *Chin. J. Electr. Eng.* **2021**, *7*, 47–54. [CrossRef]
6. Yu, C.; Zhang, X.; Liu, F.; Li, F.; Xu, H.; Cao, R.; Ni, H. Modeling and Resonance Analysis of Multiparallel Inverters System Under Asynchronous Carriers Conditions. *IEEE Trans. Power Electron.* **2017**, *32*, 3192–3205. [CrossRef]
7. Liu, H.; Xie, X. Impedance Network Modeling and Quantitative Stability Analysis of Sub-/Super-Synchronous Oscillations for Large-Scale Wind Power Systems. *IEEE Access* **2018**, *6*, 34431–34438. [CrossRef]
8. Harnefors, L.; Wang, X.; Yepes, A.G.; Blaabjerg, F. Passivity-Based Stability Assessment of Grid-Connected VSCs—An Overview. *IEEE J. Emerg. Sel. Topics Power Electron.* **2016**, *4*, 116–125. [CrossRef]
9. Wang, S.; Liu, Z.; Liu, J.; Boroyevich, D.; Burgos, R. Small-Signal Modeling and Stability Prediction of Parallel Droop-Controlled Inverters Based on Terminal Characteristics of Individual Inverters. *IEEE Trans. Power Electron.* **2020**, *35*, 1045–1063. [CrossRef]
10. Li, Z.; Wang, Z.; Wang, Y.; Yin, T.; Mei, N.; Yue, B.; Lei, W. Accurate Impedance Modeling and Control Strategy for Improving the Stability of DC System in Multiterminal MMC-Based DC Grid. *IEEE Trans. Power Electron.* **2020**, *35*, 10026–10049. [CrossRef]
11. Liu, Y.; Wang, Y.; Peng, Y.; Gao, K.; Li, R.; Liu, H. Parameter Tuning for Improving Interaction Stability of Grid-forming Converter and Power Grid. *Power Syst. Technol.* **2023**, *47*, 16–27. (In Chinese) [CrossRef]
12. Li, Y.; Tian, X.; Liu, C.; Su, Y. Study on Voltage Control in Distribution Network with Renewable Energy Integration. In Proceedings of the 2017 IEEE Conference on Energy Internet and Energy System Integration (EI2), IEEE, Beijing, China, 26–28 November 2017; pp. 1–5.
13. Li, Y.; Shuai, Z.; Liu, X.; Chen, Y.; Li, Z.; Hong, Y.; Shen, Z.J. Stability Analysis and Location Optimization Method for Multiconverter Power Systems Based on Nodal Admittance Matrix. *IEEE J. Emerg. Sel. Topics Power Electron.* **2021**, *9*, 529–538. [CrossRef]
14. Wang, Y.; Wang, X.; Blaabjerg, F.; Chen, Z. Harmonic Instability Assessment Using State-Space Modeling and Participation Analysis in Inverter-Fed Power Systems. *IEEE Trans. Ind. Electron.* **2017**, *64*, 806–816. [CrossRef]
15. Li, Y.; Shuai, Z.; Fang, J.; Wu, X. Application of Sensitivity in Impedance-based Stability Analysis for Converter Systems. *PROC CSEE* **2021**, *41*, 3480–3491+3673. (In Chinese) [CrossRef]
16. Liao, K.; Pang, B.; Yang, J.; He, Z. Compensation Strategy of Wideband Voltage Harmonics for Doubly-Fed Induction Generator. *IEEE Trans. Energy Convers.* **2023**, *38*, 674–684. [CrossRef]
17. Wang, X.; Harnefors, L.; Blaabjerg, F. Unified Impedance Model of Grid-Connected Voltage-Source Converters. *IEEE Trans. Power Electron.* **2018**, *33*, 1775–1787. [CrossRef]
18. Mattavelli, P.; Polo, F.; Dal Lago, F.; Saggini, S. Analysis of Control-Delay Reduction for the Improvement of UPS Voltage-Loop Bandwidth. *IEEE Trans. Ind. Electron.* **2008**, *55*, 2903–2911. [CrossRef]
19. Beza, M.; Bongiorno, M. On the Risk for Subsynchronous Control Interaction in Type 4 Based Wind Farms. *IEEE Trans. Sustain. Energy* **2019**, *10*, 1410–1418. [CrossRef]
20. Jiang, S.; Zhu, Y.; Konstantinou, G. Settling Angle-Based Stability Criterion for Power-Electronics-Dominated Power Systems. *IEEE Trans. Power Electron.* **2023**, *38*, 2972–2984. [CrossRef]
21. Wen, B.; Boroyevich, D.; Burgos, R.; Mattavelli, P.; Shen, Z. Analysis of D-Q Small-Signal Impedance of Grid-Tied Inverters. *IEEE Trans. Power Electron.* **2016**, *31*, 675–687. [CrossRef]
22. Xiong, L.; Liu, X.; Liu, Y.; Zhuo, F. Modeling and Stability Issues of Voltage-Source Converter Dominated Power Systems: A Review. *CSEE JPES* **2020**, *8*, 1530–1549. [CrossRef]
23. Roger, A.H.; Charles, R.J. *Matrix Analysis*, 2nd ed.; Cambridge University Press: Cambridge, UK, 2012.
24. Zhu, Y.; Zhao, J.; Mao, L.; Qu, K. Small-Signal Stability Criterion and Parametric Sensitivity Analysis for Multiple Grid-connected-converter System. *PROC CSEE* **2021**, *41*, 6235–6245. (In Chinese) [CrossRef]
25. Dong, X.; Xie, X. Influence of DFIG Controller Parameter on SSR under All Operation Areas. In Proceedings of the 2014 International Conference on Power System Technology, IEEE, Chengdu, China, 16–19 October 2014; pp. 2618–2622.
26. Wang, T.; Xiao, Y.; Zhang, X.; Xu, D. Impedance-Based Stability Analysis of DFIG. In Proceedings of the 2016 IEEE Energy Conversion Congress and Exposition (ECCE), IEEE, Milwaukee, WI, USA, 18–22 September 2016; pp. 1–4.